Molecular Therapy
Nucleic Acids
Original Article

The role of Sertoli cell-derived miR-143-3p in male fertility declines with age

Jinlian Liang,[1,5] Jiaxin Mei,[1,5] Derong Chen,[1,5] Ziyan Xiao,[1] Meirong Hu,[1] Siying Wei,[1] Zhaoyang Wang,[1] Rufei Huang,[1] Lu Li,[1] Tao Ye,[1] Jingxian Deng,[2] Yuan Liu,[1] Yuxin Wang,[1] Lei Zhang,[3] Yan Yang,[1,4] and Yadong Huang[1,4]

[1]Department of Cell Biology, Jinan University, Guangzhou 510632, China; [2]Department of Pharmacology, Jinan University, Guangzhou 510632, China; [3]Guangdong Provincial Institute of Biological Products and Materia Medica, Guangzhou 510632, China; [4]Guangdong Province Key Laboratory of Bioengineering Medicine, Guangzhou 510632, China

As delayed parenthood becomes more prevalent, understanding age-related testosterone decline and its impact on male fertility has gained importance. However, molecular mechanisms concerning testicular aging remain largely undiscovered. Our study highlights that miR-143-3p, present in aging Sertoli cells (SCs), is loaded into extracellular vesicles (EVs), affecting Leydig cells (LCs) and germ cells, thus disrupting testicular tissue homeostasis and spermatogenesis. Intriguingly, in SCs, transforming growth factor-β signaling promotes miR-143 precursors transcription, increasing mature miR-143-3p levels. This inhibits Smurf2, activating Smad2, and further enhancing miR-143-3p accumulation. EVs transporting miR-143-3p, originating from SCs, contribute to the age-related decline of testosterone and male fertility by targeting the luteinizing hormone receptor and retinoic acid receptor. Diminishing endogenous miR-143-3p in SCs postpones testis aging, preserving and prolonging male fertility. Thus, our study identified miR-143-3p as a key regulator of testicular function and fertility, revealing miR-143-3p as a potential therapeutic target for male abnormal sexual and reproductive function.

INTRODUCTION

The average age of first-time fathers has been increasing within industrialized countries. Similar to female reproductive health, male reproductive health declines with increasing age, albeit in a more gradual way.[1] This age-related decline in fertility can have significant implications for reproductive health. As men get older, they may experience reduced sperm quality and quantity, decreased testosterone, decreased libido, and an increased risk of infertility.[2] Furthermore, age-related decline in male fertility has been associated with an increased risk of certain health conditions, such as cardiovascular disease and prostate cancer.[3,4] Understanding the mechanisms underlying age-related decline in male fertility is therefore crucial for reproductive medicine and aging-related therapies.

Sertoli cells (SCs) are a unique type of somatic cell found within the seminiferous tubules of the testes. Their primary function is to support and regulate the process of spermatogenesis, which occurs within these tubules. This intricate process involves the delicate balance between the self-renewal and differentiation of spermatogonial stem cells (SSCs).[5,6] SCs create a favorable testicular microenvironment by providing physical support, maintaining structural integrity, and supplying essential nutrients to developing germ cells.[7,8] These crucial roles ensure the proper maturation of germ cells into fully functional spermatozoa. Nagano and colleagues transplanted SSCs from young male mice into the testes of both young and aged mice. After 2 months, they found that the SSCs regenerated spermatogenesis in the testes of the young recipients, but not in the aged recipients.[9] This indicated that the testicular somatic environment of aged mice may not effectively support spermatogenesis regeneration, as compared with younger mice.

In addition to supporting germ cells, SCs also play a critical role in the regulation of testosterone production and hormonal homeostasis in the testes. The production of testosterone in Leydig cells (LCs) is regulated by luteinizing hormone (LH). When LH binds to LH receptors (LHCGR) expressed in LCs, it stimulates LCs to synthesize and release testosterone. Testosterone is essential for the development and maintenance of male reproductive organs, as well as the regulation of various reproductive processes.[4,10,11] Furthermore, SCs express receptors for follicle-stimulating hormone (FSH). Upon binding to FSH, SCs initiate molecular signaling pathways that are crucial for germ cell differentiation and survival. This FSH stimulation also triggers the production and secretion of factors by SCs, such as inhibin and anti-Müllerian hormone. These factors play a role in regulating the production of testosterone by the LCs, thereby maintaining hormonal balance within the testes.[12,13] It has been reported that Sertoli cell function may decline earlier than Leydig cell function. A reduction in Sertoli cell number/proliferation at any age will therefore lead to a proportional decrease in germ cell and Leydig cell numbers,

Received 26 October 2023; accepted 24 October 2024;
https://doi.org/10.1016/j.omtn.2024.102369.

[5]These authors contributed equally

Correspondence: Yan Yang, Department of Cell Biology, Jinan University, Guangzhou 510632, China.
E-mail: yangyan107@jnu.edu.cn
Correspondence: Yadong Huang, Department of Cell Biology, Jinan University, Guangzhou 510632, China.
E-mail: tydhuang@jnu.edu.cn

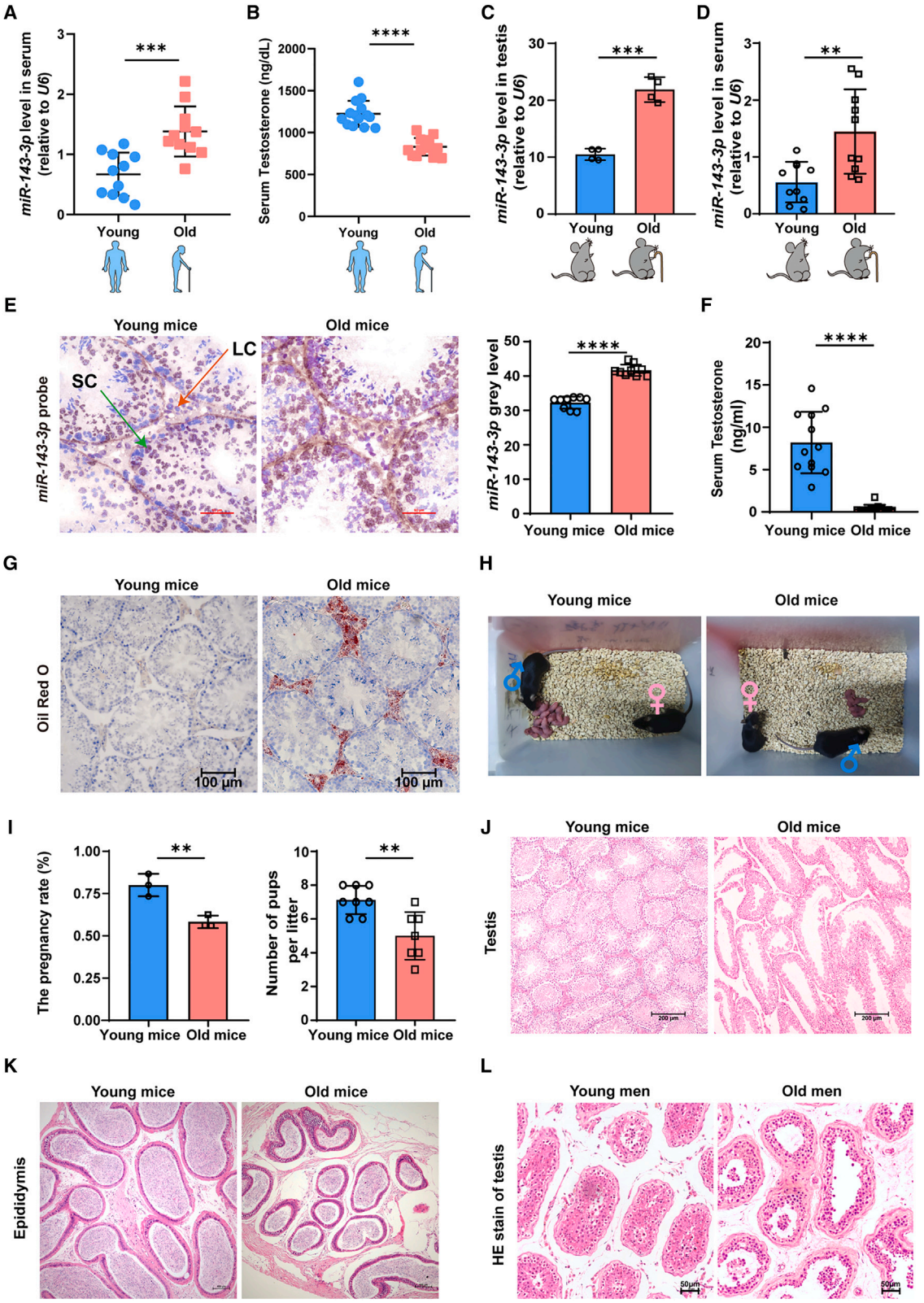

(legend on next page)

with consequential effects on fertility and health.[14] SCs are the key somatic cell population dictating the number of LCs and SSCs niches in mammalian testes.[15,16] The proper functioning of SCs is essential for overall male reproductive health. Dysregulation or dysfunction of SCs can lead to impaired spermatogenesis, decreased testosterone production, and reproductive disorders such as infertility.

Extracellular vesicles (EVs) are small membrane-bound particles released by cells into the extracellular environment. They play crucial roles in intercellular communication and cellular microenvironment[17] by carrying various bioactive molecules such as proteins, lipids, nucleic acids (including DNA, mRNA, and non-coding RNAs), and metabolites. EVs are classified into different subtypes based on their biogenesis pathways, including exosomes, microvesicles, and apoptotic bodies. They are known to carry small RNAs like microRNAs (miRNAs), which are widely studied and play substantial roles in a variety of biological or pathological processes.[18] miRNAs within EVs can be transferred to recipient cells, eliciting regulatory effects. In recent years, the role of EV-mediated intercellular communication in testes has become increasingly prominent. EVs from the reproductive tract can convey stress-related information from the paternal environment to the sperm, potentially influencing fetal development.[19,20] SCs have been identified as critical in supporting spermatogenesis through their released exosomes. These exosomes propel miRNAs such as miR-486-5p toward SSCs, instigating upregulation of genes such as Stra8, integral for germ cell differentiation.[21] Furthermore, studies have shown that exosomes from SCs can regulate Leydig cell survival via chemokine CCL20 secretion.[22] This orchestrated interaction between SCs, germ cells, and LCs through EV-derived miRNAs is vital for spermatogenesis and testicular hormone production regulation. Dysregulated EV-derived miRNAs may impair hormone signaling pathways and adversely affect male fertility. In our study, we identified that the age-related decline in testosterone levels and subfertility correlated with increased miR-143-3p expression within the testes. The exact role and regulatory mechanism of miR-143-3p in this testosterone and fertility decline, however, remain unclear.

Here, our findings revealed that the primary miR-143 (*pri-miR-143)* was strongly and exclusively expressed in aged SCs. SC-derived miR-143-3p could be transferred to LCs and SSCs via EV secretion, leading to inhibition of SSC differentiation and testosterone production both *in vitro* and *in vivo*. These findings suggested that miR-143-3p plays a crucial role in maintaining testicular microenvironment homeostasis by modulating SSC and LC functions, and may offer diagnostic markers and potential therapeutic strategies for age-related decline in fertility testosterone.

RESULTS

miR-143-3p is involved in age-associated decline of male reproductive capacity

In our study, we found that the content of miR-143-3p in serum was increased significantly in old men compared with young men (Figure 1A). The levels of serum testosterone in old men were significantly lower compared with the middle-aged and young men. Mean testosterone concentration in young men is 1182.6 ng/dL, the middle is 999.1 ng/dL, and the old is 881.7 ng/dL (Figure 1B). The miR-143-3p expression and testosterone production were inversely correlated with increasing age. We then detected the miR-143-3p in testis and serum of mice, the level of miR-143-3p was higher in the testis and serum of aged mice (18 months old) compared with young mice (3 months old) (Figures 1C–1E). Along with the increase of miR-143-3p, the testosterone level of serum also showed a dramatic drop as male mice aged (Figure 1F). In young mice, we found that the expression level of miR-143-3p was different in cells, with the highest expression in SCs, followed by SSCs and the lowest expression in LCs (Figure S1A). Furthermore, Oil Red O staining showed that elderly mice exhibited more severe lipid accumulation in the testes compared with young mice (Figure 1G), which suggested abnormal testosterone synthesis in the testes of the older mice.

As serum testosterone levels decrease, reproductive ability of aged mice undergoes changes. The fertility rates and number of pups per litter significantly decreased in aged mice (Figures 1H and 1I). Many seminiferous tubules in 18-month-old wild-type mice exhibited an "empty" appearance due to the loss of spermatogenic cells. Similar to the phenotypes observed in the seminiferous tubules (Figure 1J), most of the epididymides from 18-month-old wild-type mice showed low sperm count (Figure 1K). More important, the testes of elderly men also exhibited a similar loss of spermatogenic cells as observed in aged mice (Figure 1L).

These results indicated that testicular aging is associated with increased expression of miR-143-3p, disrupted hormonal homeostasis, and reduced spermatogenesis. This led us to question whether miR-143-3p is involved in the male age-related decline in reproductive capacity.

Figure 1. miR-143-3p involved in age-associated decline of male reproductive capacity

(A) miR-143-3p levels in serum of young, middle-aged, and old men detected by quantitative reverse-transcription PCR (n = 11). (B) Serum testosterone concentration of the young, middle-aged, and old men (n = 14) measured by radioimmunoassay (RIA). (C) Expression of miR-143-3p in testicular tissue of young and old mice detected by quantitative reverse-transcription PCR (n = 4). (D) miR-143-3p levels in serum of young and old male mice (n = 10). (E) Representative images of *in situ* hybridization of testicular tissue of young and old male mice, and the statistics results of gray values (n = 10), scale bar, 50 μm. LC was pointed out by an orange arrow and SC was pointed out by a green arrow. (F) RIA analysis of testosterone concentrations in young and old male mice serum (n = 10). (G) Representative images of Oil Red O staining in testicular tissue of young and old mice, scale bar, 100 μm. (H) Image of young and old male mice and their offspring produced after mating with female mice. (I) The pregnancy rate and number of pups produced by the young and old mice mating with female mice of appropriate age (n = 8). (J) and (K) H&E staining of testis and epididymis of young and old mice, scale bar, 200 μm and 100 μm. (L) H&E staining of testis from young and old male prostate cancer patients, scale bar, 50 μm. The data are shown as the mean ± SD; unpaired t test (A–F, I). $^{**}p < 0.01$, $^{***}p < 0.001$, $^{****}p < 0.0001$.

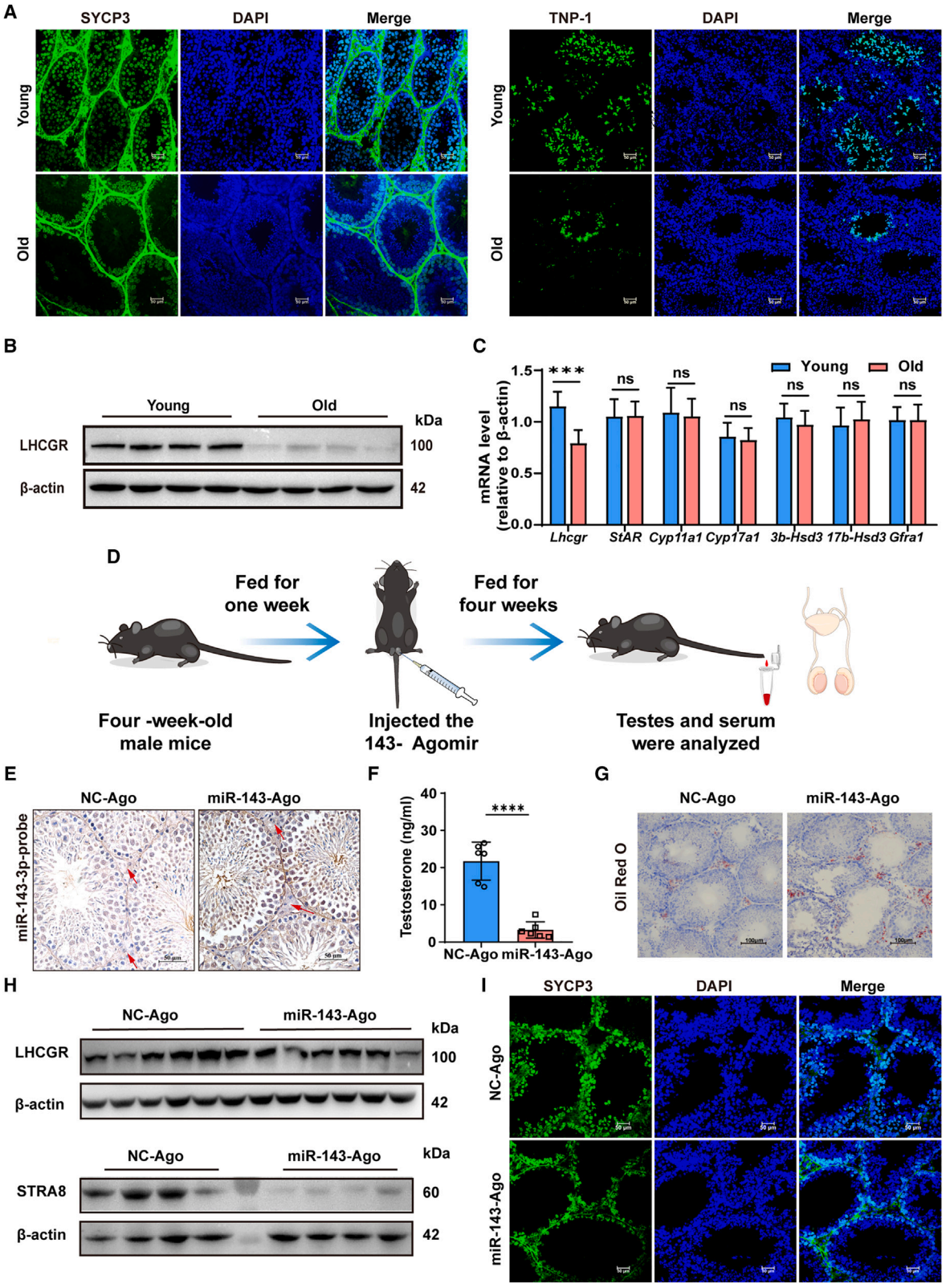

(legend on next page)

Overexpression of miR-143-3p induced testicular dysfunction in *vivo*

To investigate the potential role of miR-143-3p in age-related subfertility and reduction in testosterone levels, we first examined the expression of genes and proteins involved in the spermatogenesis and synthesis of testosterone. The number of differentiating spermatogonia expressing SYCP3 (a marker for differentiated spermatogonia) or TNP1 (a marker for differentiating spermatogonia) and LHCGR expression were significantly decreased in aged mice (Figures 2A, 2B, and S2A). In contrast, no significant change in the expression of steroidogenic-related genes (*Star*, *Cyp11a1*, *Cyp17a1*, *3b-Hsd3, 17b-Hsd3*) and *Gfra1* (a marker for A single, A paired, and A aligned spermatogonia) was observed with aging (Figure 2C).

To further examine the relationship between miR-143-3p expression and the expression of LHCGR and spermatogenesis markers, miR-143-3p agomir (a chemically modified double-strand miRNA of miR-143-3p) was injected into the interstitium of adult testes of mice, while control mice were injected with corresponding scrambled miRNAs (Figure 2D). After 4 weeks of treatment, the miR-143-3p agomir did not cause a significant increase in the number of apoptotic cells (Figures S2B and S2C), indicating that the miR-143-3p agomir did not exhibit cytotoxicity in the testes. Based on *in situ* hybridization and quantitative reverse-transcription PCR analyses, it was found that the amount of miR-143-3p was significantly increased in testis treated with miR-143-3p agomir (Figures 2E and S2D). Moreover, overexpression of miR-143-3p was associated with a decrease in the concentration of serum testosterone (Figure 2F). And there was a notable accumulation of lipid droplets accumulated in the interstitium of testes (Figures 2G and S2E), indicating that free cholesterol was not efficiently converted to testosterone. Interestingly, miR-143-3p agomir treatment also resulted in significant decreases in the levels of LHCGR, STRA8, and SYCP3 in the testis (Figures 2H, S2F, and S2G), with fewer SYCP3-positive cells observed (Figures 2I and S2H). These phenotypes were similar to those observed in testes of 18-month-old male mice, suggesting that miR-143-3p overexpression inhibited testosterone synthesis and spermatogonia differentiation.

In addition, miR-143-3p antagomir (a miR-143-3p inhibitor) was injected into the interstitium of adult testes of mice to block miR-143-3p *in vivo* (Figure S3A). The results showed that miR-143-3p antagomir upregulated the serum testosterone level of the mice (Figure S3B), reduced lipid droplets (Figure S3C), and increased the protein expressions of LHCGR, STRA8, and SYCP3 (Figures S3D and S3E). These data indicated that inhibition of miR-143-3p promoted testosterone synthesis and spermatogonia differentiation.

miR-143-3p attenuated testosterone synthesis by targeting LHCGR

To investigate the mechanism underlying how miR-143-3p inhibits testosterone production, we isolated and characterized Leydig cells (LCs) from 6-week-old mice (Figure S4A). LCs were transfected with miR-143-3p mimics, which resulted in a significant suppression of testosterone production (Figure 3A). As LH binds to the LHCGR in LCs, activating the cAMP steroidogenic pathway, cAMP production was measured. Treatment with the miR-143-3p mimic significantly inhibited cAMP production (Figure 3B). Additionally, Oil Red O staining and transmission electron microscopy (TEM) revealed an accumulation of lipids and formation of lipid droplet clusters in LCs after miR-143-3p overexpression. In contrast, LCs treated with the mimic negative control did not exhibit any obvious lipid droplet cholesterol aggregation (Figures 3C and 3D). These findings suggested that miR-143-3p overexpression interferes with cholesterol metabolism in LCs, ultimately leading to the inhibition of testosterone production.

Next, the targets of miR-143-3p in LCs were predicted. Among targets of miR-143-3p, we found that LHCGR, which exhibited significant changes in expression during mice aging, was a potential target. A potential binding site for miR-143-3p was found in the 3′ UTR of LHCGR, which is highly conserved among different species (Figure 3E). To confirm the interaction between miR-143-3p and LHCGR, a luciferase reporter assay was performed. The results showed that miR-143-3p mimic bound to the 3′ UTR site of *Lhcgr* suppressing luciferase activity. When the sequence of the 3′ UTR was mutated, the suppression was relieved (Figure 3F). In contrast, the miR-143-3p inhibitor disrupted the binding of miR-143-3p to *Lhcgr* 3′UTR rising luciferase activity (Figure S4B). Additionally, miR-143-3p mimics significantly downregulated the expression of LHCGR in LCs (Figures 3G and S4C) and miR-143-3p inhibitors dramatically upregulated the protein level of LHCGR (Figure S4D). Blocking the expression of LHCGR significantly inhibited cAMP synthesis and testosterone production, similar to the effects of the miR-143-3p mimic (Figures 3H, 3I, and S4E). Moreover, incubation with the cAMP agonist FSK effectively rescued low testosterone levels

Figure 2. Overexpression of miR-143-3p induced testicular dysfunction *in vivo*

(A) The expression of SCYP3 (green) and TNP-1 (green) in testis of different ages were detected by immunofluorescence, scale bar, 50 μm. (B) Expression level of LHCGR in young and aging mice testis ($n = 4$), and statistical analyses are shown in Figure S1A. (C) Expression of steroid-related genes (*Lhcgr, Star, Cyp11a1, Cyp17a1, 3b-Hsd3, 17b-Hsd3,* and *Gfra1*) in testis of young and old mice ($n = 6$). (D) Schematic of miR-143-3p agomir (miR-143-ago) injection into interstitium of adult mice testes ($n = 10$). (E) *In situ* hybridization was used to detect the expression of miR-143-3p after mice were injected with miR-143-3p agomir ($n = 6$), scale bar, 100 μm. (F) Serum testosterone was measured by radioimmunoassay after miR-143-3p agomir treatment ($n = 6$). (G) Representative images of Oil Red O staining for 4 weeks after miR-143-3p agomir injections, scale bar,100 μm. Statistical analyses are shown in Figure S1E. (H) LHCGR and STRA8 protein expression in testes was analyzed by western blotting for 4 weeks after miR-143-3p agomir injections, and statistical analyses are shown in Figure S1F. (I) Detection of SYCP3 (green) in testes by immunofluorescence 4 weeks after miR-143-3p agomir injection; scale bar, 50 μm. The data are shown as the mean ± SD, unpaired t test (B), (F), and (H), one-way ANOVA with multiple comparisons tests (C), ***$p < 0.001$, and ns = not significant.

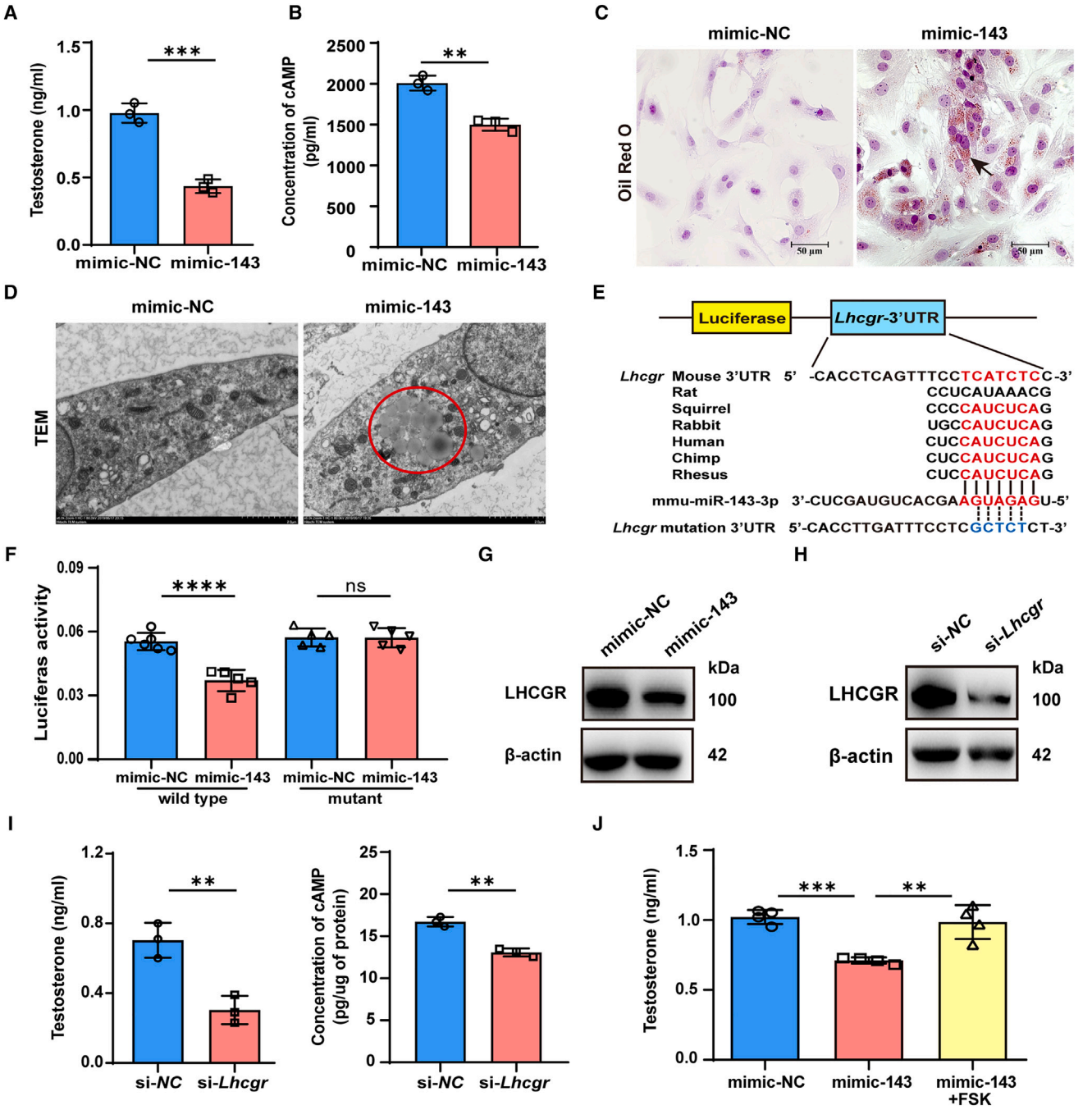

Figure 3. miR-143 attenuated testosterone synthesis by targeting LHCGR

(A) After LCs were transfected with miR-143-3p mimic (mimic-143) or NC mimic (mimic-NC) for 24 h, the complete medium was collected to detect testosterone concentration. (B) LCs transfected with miR-143-3p mimic or NC mimic for 24 h, the cells were collected to detected cAMP by ELISA. (C) Representative images of Oil Red O staining of LCs transfected with the miR-143-3p mimic or NC mimic, scale bar, 50 μm. (D) TEM images showing the formation of lipid droplet clusters in LCs overexpressing miR-143-3p, scale bar, 2 μm. (E) TargetScan predicted that miR-143-3p binds to the 3′ UTR of *Lhcgr*. (F) The wild-type and mutant vectors (Psi-Check 2 containing wild-type or 3′UTR *Lhcgr* mutant) were co-transfected with NC mimic or miR-143-3p mimic into HEK293T cells, and the relative renilla luciferase activity was measured and normalized to firefly luciferase activity. (G) LHCGR protein levels in LCs transfected with the miR-143-3p mimic. (H) The protein level of LHCGR in LCs transfected with control siRNA

(legend continued on next page)

caused by miR-143-3p mimic (Figure 3J). These findings suggest that miR-143-3p attenuated testosterone synthesis by targeting the 3′ UTR of LHCGR and inhibiting cAMP production.

miR-143-3p inhibited SSC differentiation by targeting *Rarg*

To investigate the regulatory role of miR-143-3p in SSC differentiation, the SSCs were transfected with an miR-143-3p mimic. No significant difference in GFRα-1 expression was observed (Figure 4A), suggesting miR-143-3p did not affect the maintenance of SSCs. However, overexpression of miR-143-3p significantly suppressed STRA8 and SYCP3 expression (Figures 4A and S5A). Similarly, the proportion of SYCP3-positive cells decreased after miR-143-3p mimic transfection (Figure 4B). These results suggested that miR-143-3p overexpression inhibited SSC differentiation by down-regulating STRA8 and SYCP3 expression.

We then predicted potential targets of miR-143-3p involved in regulating SSC meiosis, identifying retinoic acid (RA) receptor RARg as a candidate target. Luciferase reporter assays confirmed that miR-143-3p bound to the 3′UTR of *Rarg* (Figure 4C). In contrast, the miR-143-3p inhibitor disrupted the binding of miR-143-3p to *Rarg* 3′UTR rising luciferase activity (Figure S5B). Overexpression of miR-143-3p downregulated RARg expression (Figures 4D and S5C). Similar to the effects of the miR-143-3p mimic, blocking the expression of RARg significantly inhibited STRA8 and SYCP3 expression (Figures 4E and S5D), and reduced the proportion of SYCP3-positive cells (Figures 4F and S5E).

RARg is one receptor of RA, and to investigate its role in the regulation of SSC differentiation, we added exogenous RA to stimulate the response of RARg and compared the response of RA by the SSCs transfected with miR-143-3p. We found that the expression of SYCP3 was significantly upregulated after SSCs stimulated with RA. In contrast, exogenous overexpression of miR-143-3p inhibited RA binding to RARg, thereby decreasing SYCP3 expression (Figures 4G and S5F). These results suggested that miR-143-3p inhibited SSC differentiation by targeting *Rarg*.

EVs mediate the transfer of miR-143-3p from SCs to both LCs and SSCs

MiR-143-3p was observed to be abnormally highly expressed in the testis of aged mice, particularly in SCs (Figure 5A). To investigate the origin of miR-143-3p in LCs and SSCs, SCs were co-cultured with LCs and SSCs for 48 h, respectively. We found the amount of mature miR-143-3p in either LCs or SSCs was significantly upregulated in the same pattern after being co-cultured with SCs (Figure 5B), but this effect was blunted when SCs were treated with the EV inhibitor GW4869 (Figure 5B). However, no differences in *pri-miR-143* levels were detected (Figure 5C). This suggested that mature miR-143-3p may be generated from SCs and delivered to LCs and SSCs by EVs. EVs are particles that are released by cells and encase lipid bilayers, which are important mediators of intercellular communication. Additionally, to further determine whether miR-143-3p transfer was mediated by the release of SC-derived EVs, we co-cultured SCs with either LCs or SSCs, where the cells were separated by a membrane of 0.4 μm pore size to prevent direct cell contact or transfer of larger vesicles. FAM-labeled miR-143-3p-transfected SCs were placed in the upper chamber of a transwell co-culture system. Either LCs or SSCs were seeded in the lower chamber (Figure 5D). FAM-labeled-miR-143-3p in either LCs or SSCs was also significantly increased when SCs were cultured with either LCs or SSCs (Figures 5E and S6A), suggesting that EVs mediated the transfer of mature miR-143 from SCs to either LCs or SSCs.

We then isolated EVs from both young and old SCs, and confirmed their identity and purity through various methods. TEM and nanoparticle tracking analysis (NTA) revealed a typical cup or sphere-shaped morphology, with a size range of approximately 80–140 nm (Figures 5F and 5G). Western blot analysis showed enrichment of exosomal surface markers CD63 and CD81, while the endoplasmic reticulum marker Calnexin was not detected, confirming these vesicles were EVs (Figure 5H).

The expression level of miR-143-3p in EVs derived from old SCs was found to be significantly higher than that in EVs derived from young SCs (Figure 5I). When we added EVs derived from old SCs (old SC-Ev) into cultured LCs and SSCs, we observed a significant decrease in the level of LHCGR (target protein of miR-143-3p) in the LCs (Figure 5J). These findings suggested that the observed increase in miR-143-3p levels in recipient cells was due to EV-mediated transfer of miR-143-3p from SCs to LCs and SSCs, rather than induction of endogenous miR-143-3p expression in the recipient cells.

TGF-β induces the enrichment of miR-143-3p in SCs

Next, we explored the manner in which miR-143-3p expression is regulated during SC senescence. We found that compared with young mice, TGF-β1 levels were significantly increased in old mice (Figures 6A and S6B) and TGF-β1 induced an increase in the expression of primary miR-143 (*pri-miR-143*) and mature miR-143-3p in SCs (Figure 6B). Additionally, treatment of SCs with SB431542 (SB4), a specific inhibitor of the TGF-β receptor ALK5, completely abolished the induction of miR-143-3p (Figure 6B). Similarly, TGF-β1 increased the expression of mature miR-143-3p and SB431542 inhibited the levels (Figure 6C) in EVs from SCs. These results suggested that TGF-β1 signaling positively regulates transcription of miR-143.

(si-*NC*) or *Lhcgr* siRNA (si-*Lhcgr*) for 48 h. Statistical data are shown in Figures S2A and S2B. (I) After LCs were transfected with *Lhcgr* siRNA for 24 h, LC culture supernatant was collected to test testosterone by RIA, and LC was collected to detected cAMP by ELISA. (J) Testosterone concentration of LCs co-treated with the FSK (5 μM) and miR-143-3p or NC mimic for 48 h. The data are presented as the mean ± SD of at least three independent experiments, unpaired t test (A), (B), (G), (H), and (I); one-way ANOVA with multiple comparisons tests (F) and (J); $^{**}p < 0.01$, $^{***}p < 0.001$, $^{****}p < 0.0001$, and ns = not significant.

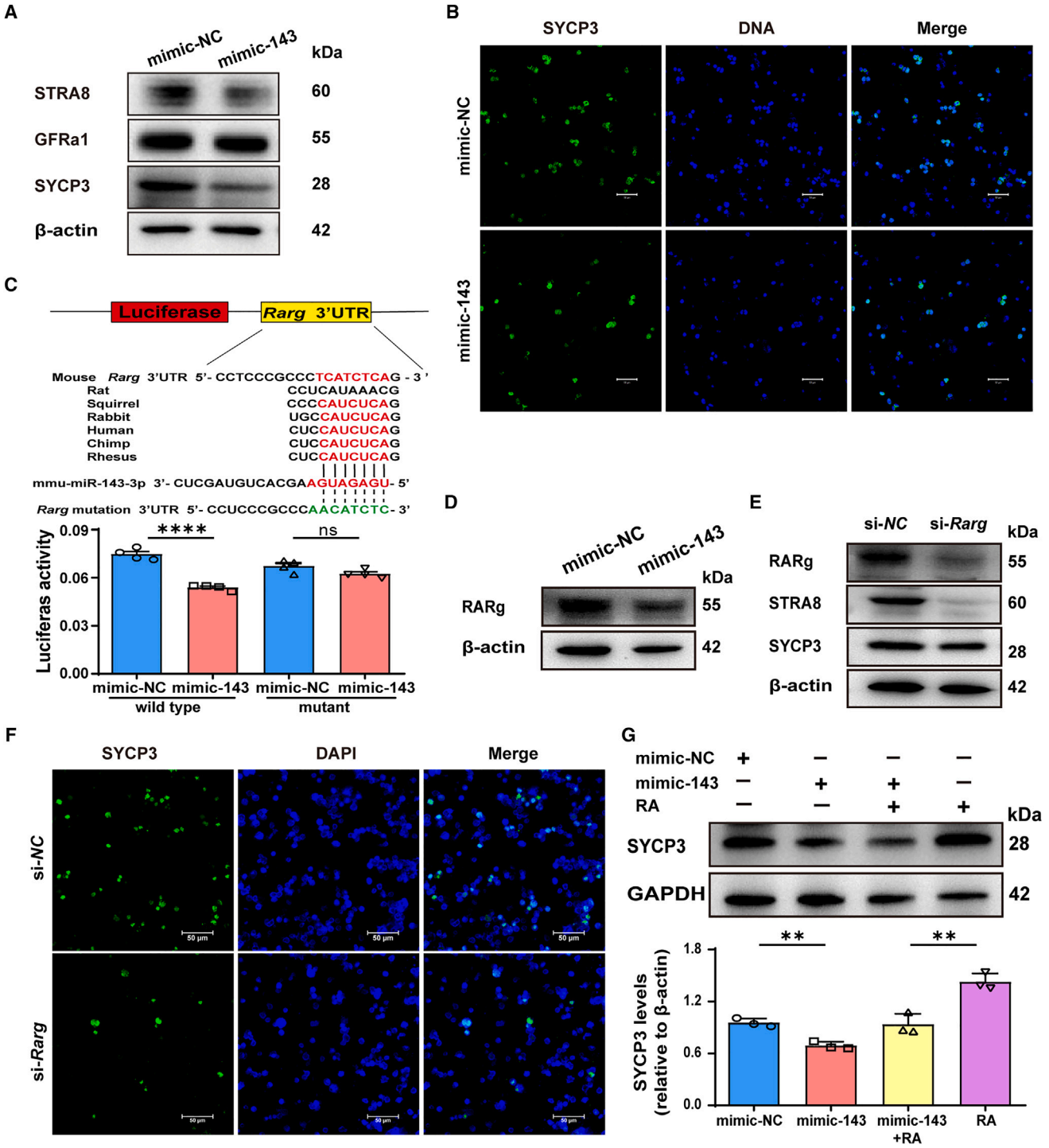

Figure 4. miR-143-3p inhibited SSCs differentiation by targeting *Rarg*

(A) The protein expressions of STRA8, GFRα1, and SYCP3 after miR-143-3p overexpression in spermatogonial stem cells (SSCs) were detected. Statistical data are shown in Figure S5A. (B) Detection of SYCP3 (green) in SSCs transfected with the miR-143-3p mimic or NC mimic by immunofluorescence, mimic-NC = simulated negative control. Scale bars, 50 μm. (C) TargetScan predicted that miR-143-3p binds to the 3′ UTR of *Rarg*. The wild-type and mutant vectors (Psi-Check 2 containing wild-type or 3′UTR *Rarg* mutant) were co-transfected with NC mimic or miR-143-3p mimic into HEK293T cells, and the relative renilla luciferase activity was measured and normalized to firefly luciferase activity. (D) RARg protein levels in SSCs transfected with the miR-143-3p mimic. The statistics are shown in Figure S5C. (E) The protein level of RARg, STRA8, and

(legend continued on next page)

In the TGF-β1 signaling pathway, TGF-β1 binds to transmembrane receptors, which in turn activates the Smads. In the nucleus, the Smad complex interplays with DNA to control gene expression. In SCs, we found that TGFβ1 increased the protein level of phosphorated Smad2 (*p*-Smad2) and had no obvious influence on Smad3 and Smad2 (Figure S6C), indicating that TGF-β1 plays a role in transcriptional regulation by activating Smad2 in SCs. To gain insight into the mechanism of miR-143 transcription regulation, we analyzed the *pri-miR-143* promoter. Our findings suggested that Smad2 may function as a transcription factor that binds to the promoter of the miR-143 gene. Overexpression of Smad2 significantly increased the expression of miR-143-3p (Figure 6D). We identified two putative Smad2 response elements within the 1.5-kb sequence of the miR-143 promoter at positions (−850) and (−568) through the Database: JASPAR (Figure 6E). To investigate the functional significance of these sites, we generated luciferase reporter constructs driven by the miR-143 promoter, with or without a mutated Smad2 binding site (Figure 6F). Notably, luciferase activity was strongly decreased in cells when the site at position (−850) were mutated, and the activity of the promoter was enhanced when the sites at position (−568) were mutated (Figure 6G), indicating that the site (−850) is necessary for TGF-β-dependent induction of miR-143. Our results demonstrated that TGF-β signaling may activated miR-143 expression, and the Smad2 could bound to the promoter of miR-143 and subsequently initiated miR-143 transcription.

miR-143-3p mediated feedback loop that directly regulates the Smad2 by targeting *Smurf2*

Interestingly, we also observed miR-143-3p overexpression resulted in an increase in Smad2 phosphorylation in SCs, while inhibition of miR-143-3p led to a decrease in Smad2 phosphorylation (Figures 7A and 7B). These findings suggested that miR-143-3p may have a positive effect on the transcription of its own precursor.

We then found that Smurf2, which functions as a negative regulator of the TGF-β signaling pathway by degrading phosphorylated Smad2, is downregulated by miR-143-3p overexpression. In contrast, the miR-143-3p inhibitor led to a significant increase in Smurf2 expression and decrease in phosphorylated Smad2 (Figures 7C and 7D). To further investigated whether Smurf2 is a direct target of miR-143-3p, we inserted the 3′UTR of *Smurf2* downstream of a luciferase reporter and co-transfected it with miR-143-3p constructs (Figure 7E). Our results showed that miR-143-3p mimics inhibited reporter activity, while mutations on the 3′UTR relieved this suppression (Figure 7F). These findings suggested that miR-143-3p suppressed *Smurf2* translation by binding to the 3′-UTR of *Smurf2*, leading to enhanced activation of Smad-dependent TGF-β signaling. This subsequently activated the transcription of *pri-miR-143*, leading to accumulation of miR-143-3p (Figure 7G).

These results suggested that TGFβ activation promotes the transcription of miR-143 precursors, leading to an increase in mature miR-143-3p. miR-143-3p then inhibited Smurf2, which activates Smad2, further increasing the accumulation of miR-143-3p. This creates a positive feedback loop that drives the continuous accumulation of miR-143-3p, ultimately exacerbating the effects of the loop.

Deletion of miR-143 in SCs alleviates male reproductive aging

To investigate the specific role of miR-143-3p derived from SCs in testis aging, we utilized Amh-Cre: miR-143 fL/fL (miR-143 conditional knockout, miR-143 CKO) mice to delete miR-143 specifically in SCs (Figure 8A). MiR-143 CKO mice were physically identical to the wild-type mice (Figure 8B). The size of testes between the two has no significant difference. This approach resulted in a reduction of miR-143-3p levels specifically in Sertoli cells (Figures S7A and S7B).

Though levels of testosterone and overall anatomical structure of seminal vesicles did not differ between 4-month-old wild-type and miR-143 CKO (Figures S7C–S7G). The testosterone levels were significantly higher in 20-month-old miR-143 CKO mice compared with age-matched wild-type mice (Figure 8C), and the expression of miR-143-3p remained at a significantly low level (Figure S8A). We then evaluated the physical performance of wild-type and miR-143 knockout mice using a series of functional assays. Results showed that, compared with 20-month-old wild-type mice, miR-143 CKO mice had a significantly increased grip strength and maximal rotarod time in age-matched mice, without a significant effect on body weight (Figures 8D and 8E). These findings suggested that increasing testosterone levels in aging mice may improve their overall health and physical activity.

Furthermore, the testes of 20-month-old wild-type mice appeared atrophic and weighed less than those of miR-143 CKO (Figure 8F). The epithelium of the seminal vesicles in wild-type mice showed irregularities, with spaces separating the epithelium and the liquid compartment. In contrast, the seminal vesicle epithelial cells from age-matched 143-knockout mice were tightly packed, similar to young mice. Additionally, many of the seminiferous tubules in wild-type mice had lost their cells, giving them an “empty” appearance, while over 90% of the seminiferous tubules from 143-knockout mice still appeared normal (Figure 8G). Additionally, although no significant changes were observed in the expression of steroidogenic genes between wild-type and 143-knockout mice (Figure S8B), the expression of LHCGR, RARg, STRA8, and SYCP3, the

SYCP3 in SSCs transfected with control siRNA (siRNA-NC), *Rarg* siRNA (siRNA-*Rarg*) for 48 h. The statistical data are shown in Figure S5D. (F) Protein level of RARg (green) detected by immunofluorescence in SSCs transfected with siRNA-NC and siRNA-*Rarg* for 48 h, scale bars, 50 μm. Fluorescence statistics are shown in Figure S5E. (G) Protein levels and the result of RARg in SSCs co-transfected with the RA and miR-143-3p or NC mimic for 48 h, β-actin was used as the internal reference. The data are shown as the mean ± SD of at least three independent experiments, unpaired t test (A), (D), and (E), one-way ANOVA with multiple comparisons tests (C) and (G). $^{**}p < 0.01$, $^{****}p < 0.0001$, and ns = not significant.

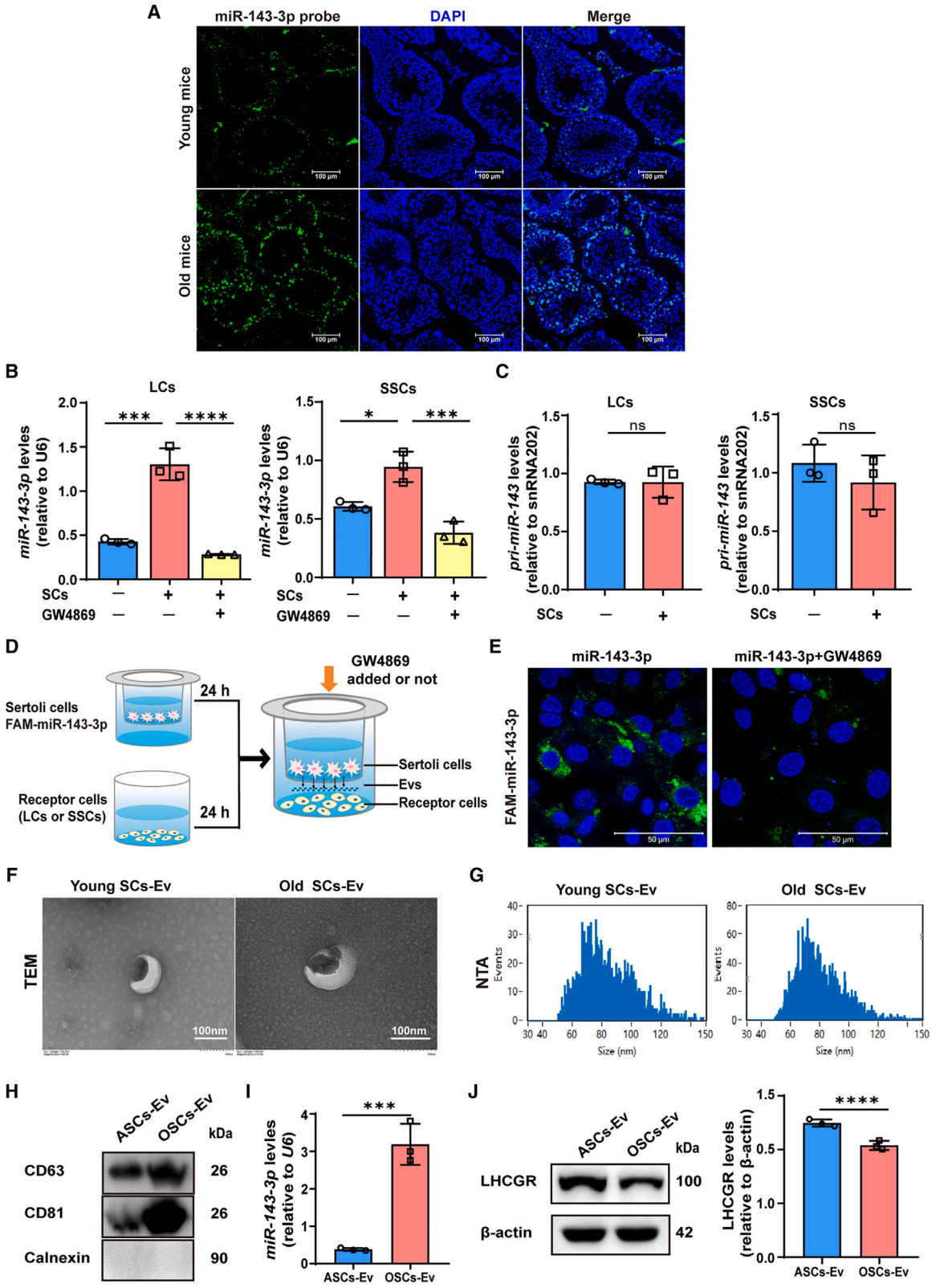

(legend on next page)

targets of miR-143-3p in the testes of 20-month-old miR-143 CKO male mice, were significantly higher than those in age-matched wild-type mice (Figures 8H and S8C). The number of SYCP3-positive spermatogonia was reduced in wild-type male mice compared with age-matched miR-143 CKO mice at the age of 20 months (Figure S8D), suggesting that the differentiating spermatogonia population is larger in miR-143 CKO male mice than in wild-type male mice in aging.

Moreover, compared with wild-type mice, miR-143 CKO mice also exhibited significantly different phenotypes in their epididymides. Most of the epididymides from 20-month-old wild-type mice had few sperm, whereas most of the epididymides of age-matched miR-143 CKO mice were full of sperm (Figure S8E). Moreover, miR-143 CKO mice had a higher total sperm count per ejaculate, as well as a higher percentage of sperm viability and progressively motile sperm with normal morphology (Figure 8I). Interestingly, sperm concentration did not decline with increasing age in miR-143 CKO mice.

To examine the reproductive system of aged miR-143 CKO mice and their fertility, we conducted breeding experiments by mating 20-month-old male mice with pairs of 10-week-old wild-type female mice. Out of the five (40%) wild-type male mice, two mice successfully sired pups, while five out of five (100%) 143-knockout males remained fertile (Figures 8J, 8K, and S8F).

These findings indicated that the reproductive organs of miR-143 CKO mice maintain a more youthful morphology and function compared with age-matched wild-type mice even into advanced age, suggesting that inhibition of miR-143 plays a crucial role in alleviating testis aging.

DISCUSSION

Aging is often accompanied by decline in testosterone levels and decreased fertility,[3,4,23] which have a negative impact on pregnancy outcomes and child development, both in natural conception and assisted reproductive techniques.[3,24] The testicular somatic cells are important components of the testicular microenvironment, which play a critical role in regulating testicular function and spermatogenesis.[16] We found that no other steroidogenic genes other than LHCGR were downregulated in aged mouse testes. It has been reported that the expression levels of steroidogenic genes such as StAR, CYP11A1, CYP17A1, 3β-HSD2, and 17β-HSD3 were not significantly different in human testis at different ages,[25] indicating that LHCGR is a key target of aging-induced testosterone decline.

EVs have emerged as important mediators of the effects of senescent cells on their microenvironment.[17] EV-derived miRNAs have been proposed as a non-invasive approach to diagnose diseases or monitor treatment efficacy.[17,18,26] Our study revealed a correlation between above-normal levels of miR-143-3p in the blood of elderly men and serum testosterone deficiency. Deletion of miR-143-3p in SCs prevented the decline of age-related testosterone and subfertility, highlighting the importance of miR-143-3p-containing EVs in maintaining testicular microenvironment homeostasis and spermatogenesis. Additionally, the levels of miR-143-3p in serum were positively correlated with those in the testis, indicating that circulating miR-143-3p may serve as a diagnostic and monitoring marker for age-related reproductive dysfunction. These findings suggest the potential utility of miR-143-3p as biomarkers for reproductive dysfunction.

SCs play important roles in mammalian spermatogenesis and testicular function. It has been reported that in men during aging, the decline in Sertoli cell function occurs earlier than the decline in Leydig cell function.[27] A reduction in Sertoli cell number or proliferation at any age can lead to a proportional decrease in germ cell and Leydig cell numbers, ultimately impacting fertility and overall health.[28] Our results demonstrate that *pri-miR-143* expression was significantly higher in SCs from aged mice, suggesting that SCs play a critical role in age-related testicular dysfunction and impaired spermatogenesis. The miR-143-3p has been reported to be involved in various biological processes such as cell proliferation,[29,30] differentiation,[31,32] apoptosis,[33] and autophagy.[34,35] In the reproductive system, miR-143-3p is highly enriched in the mouse ovary and has been shown to negatively regulate granulosa cell proliferation, cell cycle-related gene expression, and steroid hormone synthesis.[36] However, its role in the testis is still not fully understood and requires further investigation.

Our results showed that miR-143-3p targets the *Lhcgr* gene, inhibiting testosterone synthesis in LCs and aberrant expression of LHCGR contributed to aging-associated decline in testosterone. LHCGR

Figure 5. EVs mediate the transfer of miR-143-3p from Sertoli cells to both Leydig cells and SSCs

(A) Detection of the expression of miR-143-3p (green) in testis of young and old mice, scale bars, 100 μm. (B) Quantitative reverse-transcription PCR was used to detect the expression of miR-143-3p in LCs or SSCs co-cultured with SCs in medium with or without GW4869 for 48 h. Untreated LCs and SSCs were used as the control. (C) The *pri-miR-143* expression in LCs and SSCs co-cultured with SCs for 48 h were measured by quantitative reverse-transcription PCR. Untreated LCs and SSCs were used as the control. Taqman probe of *pri-miR-143* was synthesized by Thermo Fisher Scientific (assay ID: Mm03306564_pri). (D) Schematic of the co-culture system of LCs or SSCs with SCs transfected with FAM-labeled miR-143-3p. SCs transfected with FAM-labeled miR-143-3p were plated in the upper chamber of transwell culture plates, and LCs or SSCs were plated in the lower chamber. (E) Representative fluorescence images of FAM-labeled miR-143-3p (green) in LCs. SCs were transfected with FAM-labeled miR-143-3p for 24 h, then co-cultured with LCs for 48 h in medium with or without GW4869, scale bars, 50 μm. (F) Transmission electron microscopy of images of EVs isolated from the culture supernatant of young SCs and old SCs, scale bars, 100 nm. (G) NTA was used to evaluate the size distribution of EVs secreted by young and old SCS. (H) Western blot analysis of EV markers (CD63 and CD81) and Calnexin in EVs secreted by adult SCs (ASCs-Ev) or old SCs (OSCs-Ev). (I) The expression level of miR-143-3p in EVs (9.0×10^9 particles) from young and old SCs determined by quantitative reverse-transcription PCR. (J) LHCGR protein levels and the statistics in LCs treated with EVs (~3.0×10^8 particles/mL) from the young or old SCs. The presented data are the mean ± SD of at least three independent experiments, unpaired t test (E), (H), (I), and (J), one-way ANOVA with multiple comparisons tests (D). $^*p < 0.5$, $^{***}p < 0.001$, $^{****}p < 0.0001$, and ns = not significant.

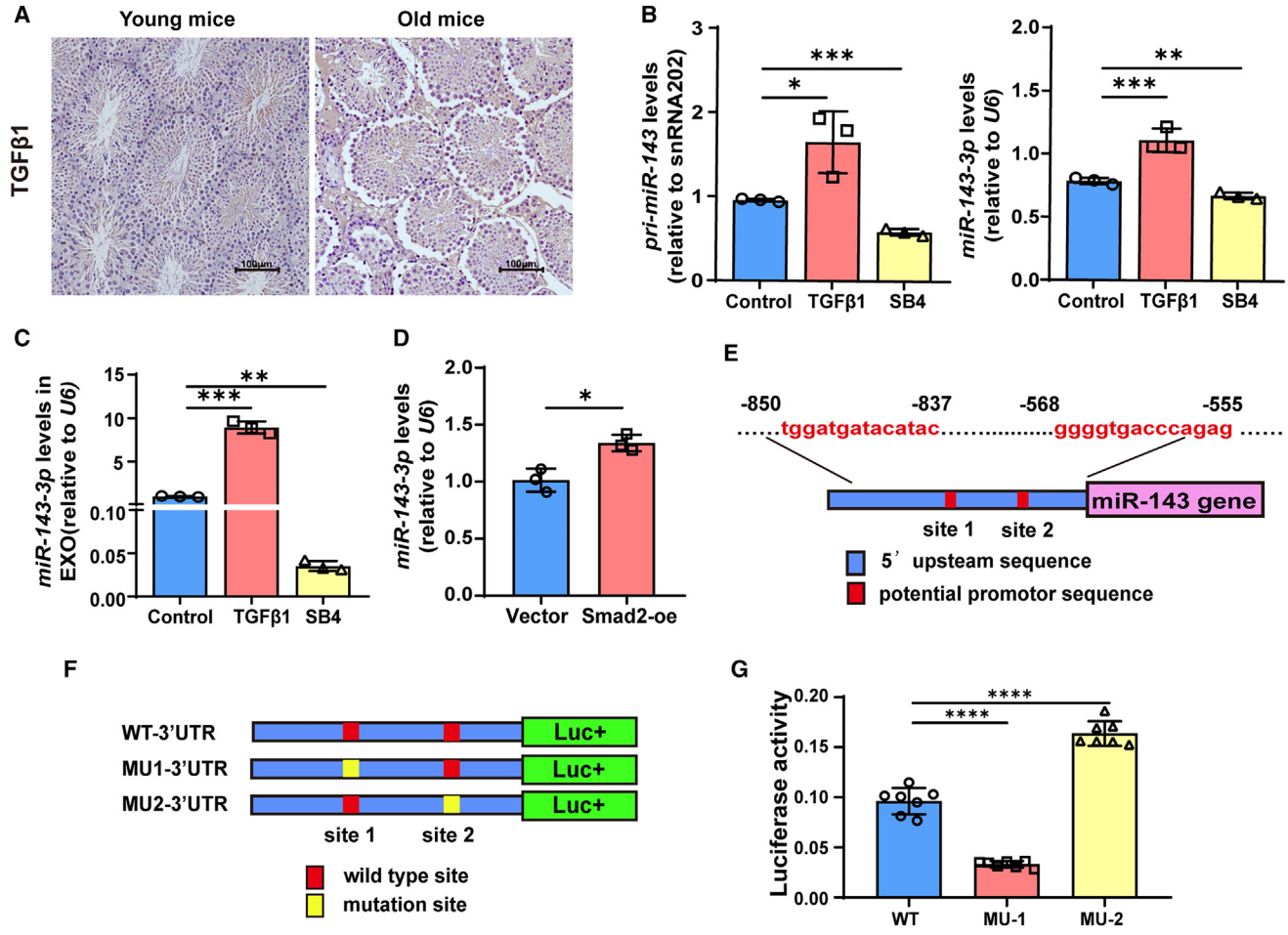

Figure 6. TGF-β triggers the transcription of miR-143 in Sertoli cells

(A) *In situ* hybridization images show TGF-β1 expression in the testis of young and aged mice, scale bar, 100 μm. (B) The mRNA levels of *pri-miR-143* and miR-143-3p in primary SCs treated with TGFβ1 (5 ng/mL) or SB431542 (2 μM) for 24 h. (C) The expression of miR-143-3p in EVs of primary SCs treated with TGF-β1 and SB431542 for 24 h. (D) miR-143-3p was detected after overexpression of Smad2 in SCs by quantitative reverse-transcription PCR. (E) and (F) Schematic diagram of potential binding sites of Smad2 in miR-143 gene and mutation in the 5′ upstream region sequence of miR-143 recombined to PGL-3 basic vector. It was used to study the promoter motif of miR-143. (G) The luciferase reporter vector and PRL-TK vector were co-transfected with Smad2 overexpression vector in HEK293T cells for 48 h. The relative luciferase activity of firefly was measured and normalized to renilla luciferase activity. Data are presented as the mean ± SD of at least three independent experiments, unpaired t test (D), one-way ANOVA with multiple comparisons tests (B), (C), and (G). $^{*}p < 0.5$, $^{**}p < 0.01$, $^{***}p < 0.001$, $^{****}p < 0.0001$.

mutations can lead to receptor inactivation due to abnormalities in receptor trafficking and signaling. Previous studies have indicated that deficiency in LHCGR can lead to a reduction in differentiating spermatogonia.[37–39] Due to the diversity of miRNA targets, although we demonstrated a targeting relationship between miR-143-3p and LHCGR, miR-143-3p still has the possibility of regulating other genes to cause different phenotypes. Our study also observed that miR-143-3p played a role in inhibiting spermatogenesis by targeting *Rarg*, which is involved in the meiotic initiation process of both sexes and is expressed by A aligned (Aal) spermatogonia, as well as during the transition from Aal to A1 spermatogonia.[40] RARg requires RA as a ligand, which binds to RA response elements in the promoter regions of the target gene *Stra8*.[41] The ablation of RARg can impair the Aal to A1 transition in some seminiferous epithelium cycles.[42] Our findings suggested that the overexpression of miR-143-3p inhibits the binding of RA to RARg, thereby reducing SYCP3 expression and ultimately inhibiting SSC differentiation by targeting RARg. These results suggested miR-143-3p plays important roles in the age-related decline of reproductive capacity.

To investigate the regulatory mechanisms underlying the age-related increase of miR-143-3p in the testis of mice, we examined the expression of both primary miR-143 (*pri-miR-143*) and mature miR-143. Our results showed that TGF-β signaling activated *pri-miR-143* expression in a Smad-dependent manner. Specifically, Smad2 was found to bind to the promoter of miR-143 gene and initiate

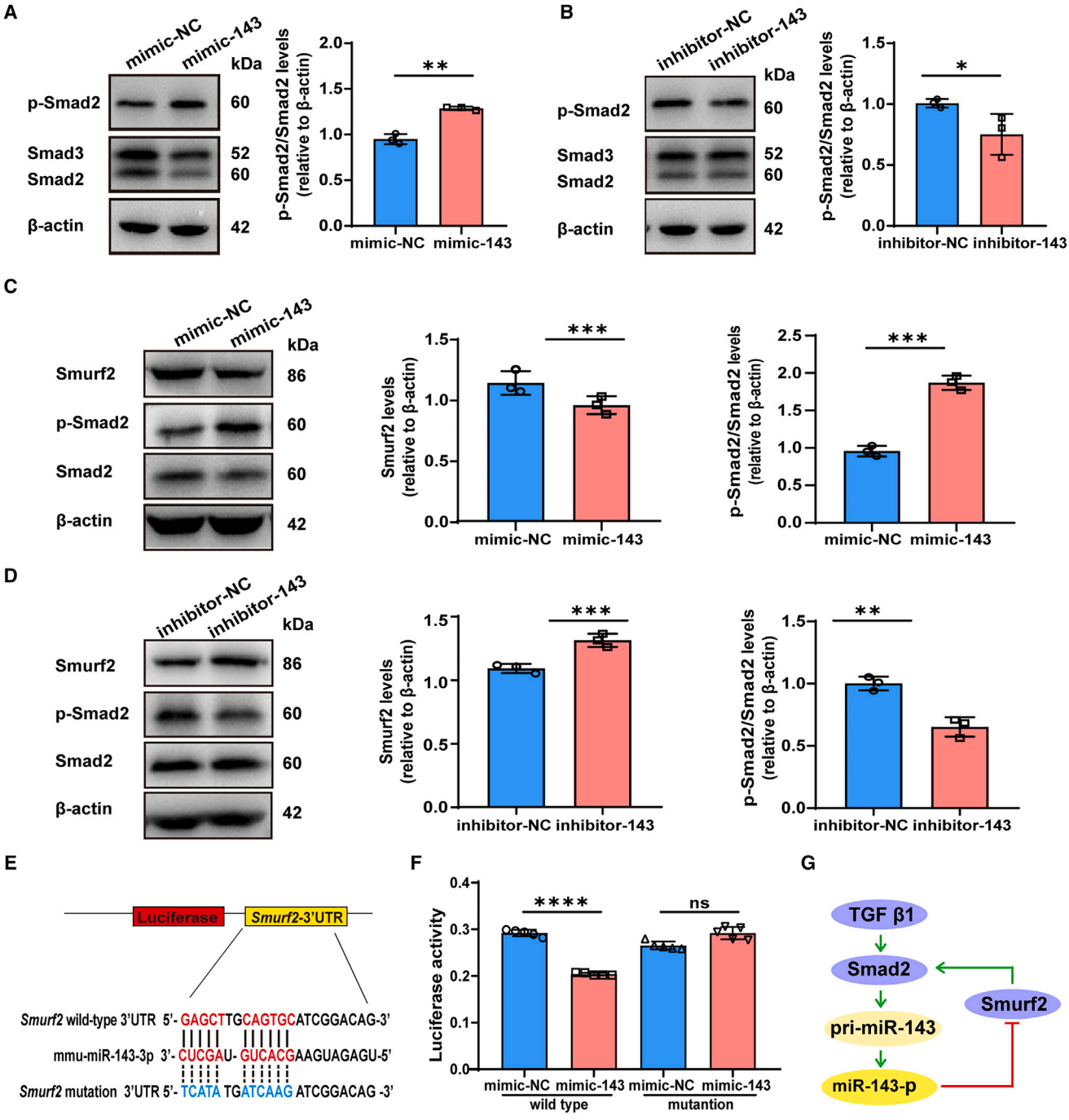

Figure 7. miR-143-mediated feedback loop that directly regulates the Smad2 by targeting *Smurf2*

(A) The protein level of *p*-Smad2, Smad2, and Smad3 in SCs transfected with mimic of miR-143-3p for 48 h. (B) The protein level of *p*-Smad2, Smad2, and Smad3 in SCs transfected with inhibitor of miR-143-3p for 48 h. (C) Expression of Smurf2, *p*-Smad2, and Smad2 in SCs transfected with miR-143-3p mimic for 48 h. (D) The protein levels of Smurf2, *p*-Smad2, and Smad2 in SCs transfected with miR-143-3p inhibitor for 48 h. (E) and (F) TargetScan predicted that miR-143-3p binds to the 3′ UTR of *Smurf2*. The wild-type and mutant vectors (Psi-Check 2 containing wild-type or 3′UTR *Smurf2* mutant) were co-transfected with mimic-NC or miR-143-3p mimic into HEK293T cells, and the relative renilla luciferase activity was measured and normalized to firefly luciferase activity. (G) Schematic diagram of Smurf2/Smad2/miR-143-3P loop regulation expression. Data are presented as the mean ± SD of at least three independent experiments, unpaired t test (A–D), one-way ANOVA with multiple comparisons tests (F). $^{*}p < 0.5$, $^{**}p < 0.01$, $^{***}p < 0.001$, $^{****}p < 0.0001$, and ns = not significant.

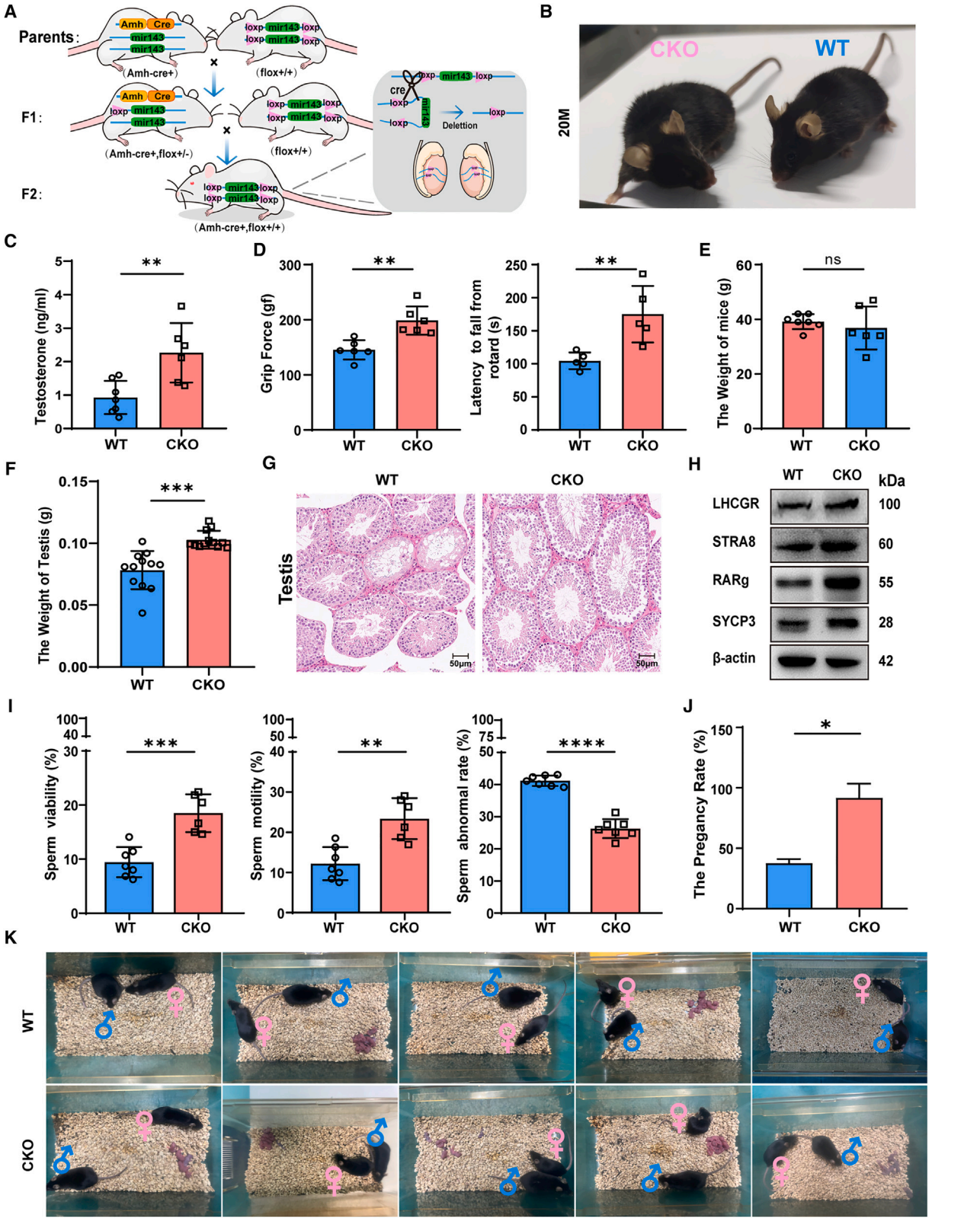

(legend on next page)

miR-143 transcription. TGF-β1 has been reported to play a role in a broad range of biological processes, including development, cell death and maintenance, aging, and disease.[43–45] In the context of reproductive aging, TGF-β signaling has been shown to regulate oocyte and germline quality maintenance.[46] In our study, we observed an age-related increase in TGF-β1 expression in the testis of old mice. TGF-β1 was found to enhance the activation of Smad2 and subsequently activate the transcription of *pri-miR-143*. miR-143-3p was then shown to inhibit the expression of Smurf2, leading to the enhanced activation of Smad2. The continuous activation of Smad2 caused by the running of the Smurf2/Smad2/miR-143-3P loop could lead to the accumulation of miR-143-3p, which could, in turn, terminate the continuous inhibition of testosterone production and SSC differentiation. It may be possible to mitigate the negative effects of aging on the reproductive system by disrupting the Smurf2/Smad2/miR-143-3P loop. However, further studies are needed to fully understand the complex regulatory mechanisms involved and to evaluate the safety and efficacy of potential therapeutic interventions.

In summary, our study demonstrated the role of SCs in age-related testicular dysfunction and identified miR-143-3p as a key player in age-related decline of reproductive capacity. miR-143-3p-containing EVs secreted by SCs inhibited testosterone synthesis and SSC differentiation, contributing to age-related decline of reproductive capacity. The Smurf2/Smad2/miR-143-3P loop played a critical role in accumulation of miR-143-3p. Targeting miR-143-3p could be a potential strategy for treating age-related subfertility and reduced testosterone levels.

MATERIALS AND METHODS

Animals and treatments

Four-week-old C57BL/6 mice were purchased from the Experimental Animal Center of Guangdong Province, China. Animals were maintained under 12 h light and dark cycle at controlled temperature (24 ± 2°C) with relative humidity (50%–60%). Standard rodent diet and drinking water are free. Young mice were raised in the laboratory until 3 months of age, while old mice were raised in the laboratory until 18 months of age. All experiments were carried out accordance with the National Institute of Health Guidelines for the Care and Use of Animals and approved by the Institutional Animal Care and Use Committee(IACUC) of the Jinan University (IACUC Approval: 20210630-04).

Young and old men volunteers recruited

Sixteen young men (aged 21–29 years), 17 middle-aged men (aged 30–49 years), and 16 old men (aged 60–70 years) without underlying diseases were recruited, and 5 mL of venous blood was collected from each person before 10:00 a.m. for serum testosterone detection and circulating RNA isolation. The testicular HE staining samples used in this study were generously provided by the First Affiliated Hospital of Sun Yat-sen University. These samples were obtained from patients with prostate cancer across various age groups. All experiments were performed in accordance with institutional review board of Jinan University (JNUKY-2021-052).

Spermatogonial stem cell isolation and culture

Primary spermatogonial stem cells (SSCs) were derived from the testis of 7-day-old male mice. Testes were treated with 5 mL type IV collagenase (1 mg/mL) at 37°C for 10 min to remove LCs, Myoid cells, and blood cells. Digestion was terminated with 10 mL DMEM medium (Gibco, C11995500BT) without FBS. The suspension was centrifuged at 100 × *g* for 2 min and secondly digested with 0.25% trypsin containing 1 mmol/L EDTA (Gibco, 25200072) at 37°C for 10 min. Double volume of DMEM medium containing 10% FBS (ExCell, FSD500) was added to stop the digestion. After digestion, the cell pellets were re-suspended in complete medium. and cultured in a cell culture dish for 24 h. The SCs completely attached to the bottom of the cell dish and SSCs suspended in the medium. Then, the SSCs were collected and cultured with DMEM medium with 10% FBS.

Leydig cell and Sertoli cell isolation and culture

Primary Leydig cells (LCs)[47] and Sertoli cells (SCs) were obtained from the testis of a 6-week-old male mouse. Briefly, the testicle stripped of tunica albuginea was incubated with 1 mg/mL type IV collagenase (Biosharp, C-5138) in DMEM on a 37°C shaker for 10 min. Digestion was terminated and divided into two parts: supernatant and precipitation. The Leydig cells in suspension were collected and centrifuged at 250 × *g* for 5 min after filtering through a 40-μm cell strainer (Falcon, 352340). Cells were re-suspended in DMEM containing 10% FBS and incubated at 37°C with 5% CO_2. Subsequently, 0.25% trypsin solution was added to the precipitation for further digestion on a 37°C shaker for 15 min. The suspension was filtered through a 100-μm cell filter (Falcon, 352360) and centrifuged at 250 × *g* for 5 min to collect the digested cells and re-suspended in DMEM with 10% FBS. The cell suspension was cultured at 37°C with 5% CO_2 for 24 h, the adherent cells were collected and treated with hypotonic solution (20 mmol/L Tris, pH 7.4) for 2 min to obtain pure SCs. LCs and SCs were cultured in DMEM supplemented with 10% FBS at 37°C and 5% CO_2.

Figure 8. Deletion of miR-143 in SCs alleviates the male reproductive aging

(A) Schematic diagram of specific conditional knockout of miR-143 in SCs performed in C57 mice. (B) Representative appearance of 20-month-old wild-type (WT) and CKO mice. (C) Serum testosterone was measured by radioimmunoassay in 20-month-old WT (n = 7) and CKO (n = 6) mice. (D) Detection of motor capacity (Rotarod and Grip strength test) in WT and CKO mice (n = 6). (E) Body weight of 20-month-old WT and CKO mice (n = 6). (F) Testis weight of WT and CKO mice (n = 6). (G) H&E staining in testes of 20-month-old WT and CKO mice (n = 6). (H) The protein expression of LHCGR, STRA8, RARg, and SYCP3 in WT and CKO mouse testes, the statistical results are shown in Figure S8C. (I) Statistical results of spermatozoa detection (sperm viability, sperm motility, sperm abnormal rate) in 20-month-old WT (n = 7) and CKO (n = 6) mice. (J) Differences in fertility between WT and CKO mice. (K) Presentation of the fertility of WT and CKO mice in co-cage mating (n = 5). Data are shown as the mean ± SD, unpaired t test (C)–(F), (H)–(J), $^{*}p < 0.5$, $^{**}p < 0.01$, $^{***}p < 0.001$, $^{****}p < 0.0001$, and ns = not significant.

Cell transfection

Primary LCs (5×10^5) and SSCs (1×10^6) were respectively seeded in a six-well plate for 24 h. Thirty picomoles siRNA (miR-143 mimic, inhibitor or respective NC) was transfected to cells with 7.5 μL Lipofectamine RNAiMAX (Invitrogen, 13778150) reagent. After culturing for 24 or 48 h, the cells were collected for further analysis.

Serum RNA isolation and miR-143-3p detected

Serum was isolated from blood by centrifugating for 15 min at 3500 rpm. Trizol LS reagent (Invitrogen, 10296010) was used to extract total from 300 μL serum. The collected RNA was dissolved in 15 μL RNase free water. The quality was determined by Nanodrop 2000 (Thermo Scientific, USA), with 260/280 wavelength being in range of 1.8–2.0, and yield reaching 400–1000 ng.

The quantitative reverse-transcription PCR was performed by 2 × All-in-One qPCR kit (GeneCopoeia, QP115). The extracted RNA is polyadenylated using poly(A) polymerase. This enzyme adds a poly(A) tail to the 3′ end of RNA molecules, including microRNAs, which typically lack a poly(A) tail. The reverse-transcription PCR is performed using a poly(T) primer containing a universal adapter sequence and a specific oligo (dT) sequence. In detail, 400 ng RNA was used to synthesize cDNA in a 20-μL reaction including 4 μL 5× PAP/TR buffer, 1 μL RTase mix, and 1 μL 2.5U/μL poly A polymerase. Then performed 37°C for 60 min, and at 85°C for 5 min. Subsequently, the quantitative PCR was performed using a universal adapter primer and specific primers for miRNA-143-3p (TGAGATGAAGCACTGTAGCTCAAA). BioRad CFX manager system (BioRad, USA) was used to perform 95°C for 10 min, followed by 40 cycles of 95°C for 10 s and 60°C for 20 s and 72°C for 10 s. The relative expression of miR-143-3p was calculated by the $2^{-\Delta\Delta Ct}$ method normalized by U6.

Quantitative reverse-transcription PCR

Total RNA was extracted from EVs or cells using Trizol reagent (Invitrogen, 15596026) according to the manufacturer's instructions and levels of specific mRNA were measured by quantitative reverse-transcription PCR. Total RNA was reverse transcribed using PrimeScript RT Master Mix (Takara, RR036B). qPCR was conducted with ChamQ SYBR qPCR Master Mix (Vazyme, Q311-02) according to the manufacturer's instructions. All primers were designed by Primer-BLAST (https://blast.ncbi.nlm.nih.gov/Blast.cgi) and the primers used are described in supplemental information (Table S1). The data were normalized to β-actin or U6. The comparative $2^{-\Delta\Delta Ct}$ method was used to calculate relative gene expression.

Taqman *pri-miR-143* detected assay

The quantitative reverse-transcription PCR taqman probe and primers of *pri-miR-143* were designed by Thermo Fisher. First, 2 μg RNA was used to synthesize cDNA in a 20 μL reaction, performed 37°C for 60 min, and at 95°C for 5 min (Thermo Fisher, 4387406). Then, quantitative PCR was performed using *pri-miR-143* specific primers and taqman probe mix (Thermo Fisher, assay ID Mm03306564_pri) and TaqMan Fast Advanced Master Mix (Thermo Fisher, 4444556) with conducting 50°C for 2 min, 95°C for 20 s, followed by 40 cycles of 95°C for 3 s and 60°C for 30 s. The relative expression of *pri-miR-143* was calculated by the $2^{-\Delta\Delta Ct}$ method normalized by snRNA202.

Western blot

Cells were washed twice with phosphate buffered saline (PBS) at room temperature. RIPA lysis buffer (Fude, FD008) containing 1 mM PMSF (Fude, FD0100) and phosphatase inhibitor PhosSTOP (Roche, 4906845001) was added to the cells for 30 min in ice. Then cell lysate protein concentrations were determined by BCA Protein Assay Kit (Thermo Fisher Scientific, 23225). Thirty-microgram total protein samples were separated by electrophoresis on 10% SDS-PAGE and electro-transferred for 90 min onto PVDF membranes. Sealing with 5% skimmed milk for 60 min, antibodies (Table S2) were added and incubated overnight at 4°C. Membranes were washed five times with Tris-buffered saline containing 0.1% Tween 20 (TBST) and incubated with a horseradish peroxidase (HRP)-conjugated secondary antibody (1:5,000) at room temperature for 60 min. Membranes were washed again and protein levels were detected by enhanced chemiluminescence (ECL) kit (Fude, FD8020). The protein expression levels were normalized by β-actin.

Immunofluorescence

Cells were fixed with 4% paraformaldehyde for 10 min and washed with PBS three times. Cells were treated with 0.5% Triton X- for 10 min to increase membrane permeability. Five percent bovine serum albumin was used to blook the non-specific adhesion sites for 1 h at room temperature. The cells were incubated with primary antibodies (Table S2) at 4°C overnight and washed with PBS three times, then incubated with secondary antibodies (Abcam, Ab150077) at room temperature for 1 h. Cell nuclei were stained with 1 μg/mL DAPI solution (Boster, AR1177). The stained samples were imaged in real time with an ECLIPSE Ni-U upright microscope (Nikon) and analyzed with ImageJ software.

Co-culture assay

Co-culture experiments were carried out in a 24-mm transwell (Corning, 3412). Primary SCs were seeded in the upper chamber of the transwell and transfected with miR-143-3p (FAM) for 24 h. Primary LCs or SSCs were seeded in the down chamber for 24 h. Then, medium from the upper chamber was removed, and SCs were washed three times with PBS to remove excess miR-143-3p (FAM) probe. SCs were co-cultured with LCs or SSCs for 48 h, meanwhile, 10 μM GW4869 (MedChemExpress, HY-19363) was added to the culture system to inhibit the production of EVs.

TUNEL assay

Frozen sections of testicular tissue were taken out of the refrigerator at −80°C and returned to room temperature. Slices were soaked in 1% Triton X-100 permeable solution for 3–5 min, then washed with PBS. TdT enzyme reaction solution was added to cover the tissue, and the samples were placed in a wet box and incubated at 37°C for 60 min in the dark. In addition, DNase I reaction solution was added to the

positive group, and the reaction was carried out at 37°C for 30 min without TdT enzyme. The fluorescein markers were then added to streptavidin-fluorescein labeling solution and placed in a wet box for 30 min at 37°C under light. Finally, the nuclei were stained with DAPI and covered with fluorescence quencher. The stained samples were imaged in real time using a Nikon forward microscope.

Luciferase reporter assay

The dual-luciferase reporter plasmid and miR-143-p mimic or inhibitor were transfected into 293T or TM3 cells for 48 h. Dual-Luciferase Reporter Assay System kit (Promega, E1910) was used to detect bioluminescence. Briefly, 100 μL of Luciferase Reagent was added per well, mixed with a shaker for 15 s, and incubated at room temperature for 10 min. The fluorescence signal of firefly was detected with full-function enzyme marker and recorded. Then 100 μL of Stop & Glo Reagent was added to each well, and the above operation was repeated. The fluorescence signal of the kidney was detected 10 min later, and the data were recorded and analyzed.

EV extraction and isolation

Primary cells were cultured in T75 flasks with complete medium for 24 h. Medium was changed to DMEM containing 5% Knockout Serum Replacement (Gibco, 10828028) to eliminate the EVs from fetal bovine serum and continued to culture for 72 h. Then, the medium was collected and filtered through a 0.22-μm filter (Millipore, slgp033rb). EVs were collected by differential centrifugation. In short, the supernatant was centrifuged at 4°C as follows: 300 × *g* for 10 min, 10,000 × *g* for 30 min, and 100,000 × *g* for 70 min. For EV purification, particles were subsequently subjected to an additional washing step with PBS at 160,000 × *g* for 1 h. Finally, EVs were stored at −80°C.

Nanoparticle tracking analysis

EVs from P1 and P4 generation of SCs were thawed in a 37°C water bath and re-suspended in 70 μL PBS. Then, 10 μL of EV suspension was taken for analysis of its size and concentration using Malvern's NanoSight NS300 (England).

Transmission electron microscopy

EVs were suspended in 100 μL frozen PBS. Samples were dripped onto a copper mesh, fixed with 2.5% glutaraldehyde for 5 min, washed with deionized water 10 times, and negatively stained with 40 g/L uranyl acetate for 10 min. The copper mesh was allowed to dry naturally. Photographs were taken using an electron microscope.

Testosterone measurement

Testosterone concentrations of serum and LC culture supernatant were measured using radioimmunoassay (RIA) with iodine labeling, according to the iodine ^{125}I testosterone radioimmunoassay kit (Beijing North Institute of Biotechnology). Blood was centrifuged at 3,500 rpm for 15 min and the upper serum was collected. The cell culture supernatant was obtained from LC cells cultured in DMEM containing 10% FBS for 24 h. A 50-μL sample and a series of standard solutions (0, 0.1, 0.5, 2.0, 8.0, 20 ng/mL) were added to 5-mL test tubes, respectively. Then 100 μL of testosterone antibody was added to each tube and incubated at room temperature for 1 h. Subsequently, 500 μL ^{125}I-T reagent was added and incubated in a 37°C water bath for 1 h to competitively bind with the testosterone antibody. Next, iodine-labeled separation reagent was added and incubated for 15 min, centrifuged at 3,500 rpm for 15 min to collected precipitate. Finally, radioactivity was detected by a gamma counter. The curve was fitted according to the concentration of the standard samples and the radioactive detection values, and the testosterone concentration of the samples was calculated.

In situ hybridization of miR-143-3p

After routine dewaxing and rehydration, paraffin sections of mouse testis tissue were treated with 3% hydrogen peroxide for 5–10 min at room temperature, and pepsin containing 3% citric acid was added and digested for 15 min at room temperature, and fixed with 1% paraformaldehyde for 10 min at room temperature. Pre-hybridization solution was dripped and incubated at 42°C for 2–4 h in the wet box, and then the tissues were incubated with miR-143-3p probe (Table S3) at 42°C overnight. The unhybridized probes were washed away with saline sodium citrate and blocking solution was added to block non-specific adhesion sites for 30 min at 37°C. The tissues were then incubated with biotinylated mouse anti-digoxin at 37°C for 60 min, followed by incubation with streptavidin biotin-peroxidase complex (SABC) for 20 min, incubated with biotinylated peroxidase for 20 min, stained with DAB substrate, and washed with water. Then, tissues were dehydrated with alcohol, transparent with xylene, sealed and observed using the Nikon microscope. This customized miR-143-3p probe for detection purposes was provided by Boster.

Oil red O staining

The frozen sections of testicular tissue were washed three times in distilled water for 3 min each time, soaked in 60% isopropanol for 30 s, and then stained in modified Oil Red O staining solution for 10 min. Then the sections were washed in 60% isopropyl alcohol to remove the background staining, and stained with hematoxylin for 5 min. The sections were dried and sealed with glycerin gelatin, and then the morphology of tissue lipid droplets was observed and photographed by microscope (Nikon).

Testicular injection of miR-143-3p agonist and antagonist

After randomization of 4-week-old male C57BL/6J mice, the mice were kept for 1 week, and after anesthesia with 1% sodium pentobarbitone, 50 nmol of the miR-143-3p agomir (a double-strand miR-143-3p mimic with cholesterol and 2′OME modification), miR-143-3p antagomir or their controls were dissolved in 400 μL of PBS and slowly injected into the bilateral testis of 10 mice with 15 μL per testis. This is equivalent to 1.875 nmol siRNA per testis. These nucleic acid drugs (Table S4) were purchased from Ribobio. In addition, the sequences of miR-143-3p agomir and antagomir are listed in the Table S4.

Sperm motility quality test

One side of the cauda epididymis was taken out and placed into a 1.5-mL EP tube containing 1 mL PBS at 37°C, then, cut and incubated at

37°C for 10 min to release sperm. After the sperm were fully released, the sperm suspension was mixed thoroughly, and 10 μL of sperm suspension was aspirated to a sperm counting plate with a depth of 60 μm. The motility, viability, and number of mouse sperm were analyzed by computer-assisted semen analysis system (CASA), and malformation rate was calculated manually.

Statistical analysis

All experiments were repeated at least three times, and data were expressed as the mean ± 1 standard deviation around the mean (SD). Statistical analyses were performed by GraphPad prism 8 software. Statistical analyses were performed with an unpaired Student's t test or one-way ANOVA using Dunnett's multiple comparisons test for more than two groups. A p value <0.05 was considered statistically significant.

DATA AND CODE AVAILABILITY

The data that support the findings of this study are available from the corresponding author upon reasonable request.

ACKNOWLEDGMENTS

This research was funded by National Natural Science Foundation of China (No. U22A20277, 32170865, and 82071634); Natural Science Foundation of Guangdong Province (No. 2022A1515012178); the Science and Technology Plan Project of Guangzhou (No. 202002030168, 202102080124); Medical Scientific Research Foundation of Guangdong Province of China (No. B2020139) and Guangzhou Key R&D Program (No. 202103030003); Guangdong Key Areas R&D Program (No. 2022B1111080007).

AUTHOR CONTRIBUTIONS

Y.Y., Y.H., J.L., D.C., and J.M. conceptualized the study. J.L., D.C., and J.M. acquired and analyzed the data. Z.X., M.H., S.W., and Z.W. completed the animal experiments. R.H., L.L., T.Y., J.D., Y.L., Y.W., and L.Z. completed the illustration and manuscript proofreading. Y.Y. and Y.H. supervised the project. All authors read and approved the final manuscript.

DECLARATION OF INTERESTS

The authors declare no competing interests.

SUPPLEMENTAL INFORMATION

Supplemental information can be found online at https://doi.org/10.1016/j.omtn.2024.102369.

REFERENCES

1. Meyer, R.G., and Meyer-Ficca, M.L. (2021). Metabolism in Male Reproductive Aging. Adv. Geriatr. Med. Res. *3*, e210005.
2. Almeida, S., Rato, L., Sousa, M., Alves, M.G., and Oliveira, P.F. (2017). Fertility and Sperm Quality in the Aging Male. Curr. Pharmaceut. Des. *23*, 4429–4437.
3. Kaufman, J.M., Lapauw, B., Mahmoud, A., T'Sjoen, G., and Huhtaniemi, I.T. (2019). Aging and the Male Reproductive System. Endocr. Rev. *40*, 906–972.
4. Lunenfeld, B. (2006). Endocrinology of the aging male. Minerva Ginecol. *58*, 153–170.
5. Zhang, Q., Sun, J., Huang, Y., Bu, S., Guo, Y., Gu, T., Li, B., Wang, C., and Lai, D. (2019). Human Amniotic Epithelial Cell-Derived Exosomes Restore Ovarian Function by Transferring MicroRNAs against Apoptosis. Mol. Ther. Nucleic Acids *16*, 407–418.
6. Chen, S.R., and Liu, Y.X. (2015). Regulation of spermatogonial stem cell self-renewal and spermatocyte meiosis by Sertoli cell signaling. Reproduction *149*, R159–R167.
7. Solon-Biet, S.M., Walters, K.A., Simanainen, U.K., McMahon, A.C., Ruohonen, K., Ballard, J.W.O., Raubenheimer, D., Handelsman, D.J., Le Couteur, D.G., and Simpson, S.J. (2015). Macronutrient balance, reproductive function, and lifespan in aging mice. Proc. Natl. Acad. Sci. USA *112*, 3481–3486.
8. Oatley, M.J., Racicot, K.E., and Oatley, J.M. (2011). Sertoli cells dictate spermatogonial stem cell niches in the mouse testis. Biol. Reprod. *84*, 639–645.
9. Zhang, X., Ebata, K.T., Robaire, B., and Nagano, M.C. (2006). Aging of male germ line stem cells in mice. Biol. Reprod. *74*, 119–124.
10. Fink, J.E., Hackney, A.C., Matsumoto, M., Maekawa, T., and Horie, S. (2020). Mobility and Biomechanical Functions in the Aging Male: Testosterone and the Locomotive Syndrome. Aging Male *23*, 403–410.
11. Gunes, S., Hekim, G.N.T., Arslan, M.A., and Asci, R. (2016). Effects of aging on the male reproductive system. J. Assist. Reprod. Genet. *33*, 441–454.
12. Schlatt, S., Gassei, K., Westernströer, B., and Ehmcke, J. (2010). Modulating testicular mass in xenografting: a model to explore testis development and endocrine function. Endocrinology *151*, 4018–4023.
13. Skinner, M.K., and Griswold, M.D. (2004). Sertoli Cell Biology (Elsevier).
14. Jarak, I., Almeida, S., Carvalho, R.A., Sousa, M., Barros, A., Alves, M.G., and Oliveira, P.F. (2018). Senescence and declining reproductive potential: Insight into molecular mechanisms through testicular metabolomics. Biochim. Biophys. Acta, Mol. Basis Dis. *1864*, 3388–3396.
15. Rebourcet, D., Darbey, A., Monteiro, A., Soffientini, U., Tsai, Y.T., Handel, I., Pitetti, J.L., Nef, S., Smith, L.B., and O'Shaughnessy, P.J. (2017). Sertoli Cell Number Defines and Predicts Germ and Leydig Cell Population Sizes in the Adult Mouse Testis. Endocrinology *158*, 2955–2969.
16. Rebourcet, D., O'Shaughnessy, P.J., Pitetti, J.L., Monteiro, A., O'Hara, L., Milne, L., Tsai, Y.T., Cruickshanks, L., Riethmacher, D., Guillou, F., et al. (2014). Sertoli cells control peritubular myoid cell fate and support adult Leydig cell development in the prepubertal testis. Development *141*, 2139–2149.
17. Takasugi, M. (2018). Emerging roles of extracellular vesicles in cellular senescence and aging. Aging Cell *17*, e12734.
18. Dluzen, D.F., Noren Hooten, N., and Evans, M.K. (2017). Extracellular RNA in aging. Wiley Interdiscip. Rev. RNA *8*, e1385.
19. Chan, J.C., Morgan, C.P., Adrian Leu, N., Shetty, A., Cisse, Y.M., Nugent, B.M., Morrison, K.E., Jašarević, E., Huang, W., Kanyuch, N., et al. (2020). Reproductive tract extracellular vesicles are sufficient to transmit intergenerational stress and program neurodevelopment. Nat. Commun. *11*, 1499.
20. Yang, W., Zhang, J., Xu, B., He, Y., Liu, W., Li, J., Zhang, S., Lin, X., Su, D., Wu, T., and Li, J. (2020). HucMSC-derived exosomes mitigate the age-related retardation of fertility in female mice. Mol. Ther. *28*, 1200–1213.
21. Li, Q., Li, H., Liang, J., Mei, J., Cao, Z., Zhang, L., Luo, J., Tang, Y., Huang, R., Xia, H., et al. (2021). Sertoli cell-derived exosomal MicroRNA-486-5p regulates differentiation of spermatogonial stem cell through PTEN in mice. J. Cell Mol. Med. *25*, 3950–3962.
22. Ma, Y., Zhou, Y., Zou, S.S., Sun, Y., and Chen, X.F. (2022). Exosomes released from Sertoli cells contribute to the survival of Leydig cells through CCL20 in rats. Mol. Hum. Reprod. *28*, 1–10.
23. Ilacqua, A., Izzo, G., Emerenziani, G.P., Baldari, C., and Aversa, A. (2018). Lifestyle and fertility: the influence of stress and quality of life on male fertility. Reprod. Biol. Endocrinol. *16*, 115.
24. Yatsenko, A.N., and Turek, P.J. (2018). Reproductive genetics and the aging male. J. Assist. Reprod. Genet. *35*, 933–941.
25. Mularoni, V., Esposito, V., Di Persio, S., Vicini, E., Spadetta, G., Berloco, P., Fanelli, F., Mezzullo, M., Pagotto, U., Pelusi, C., et al. (2020). Age-related changes in human Leydig cell status. Hum. Reprod. *35*, 2663–2676.
26. Robbins, P.D. (2017). Extracellular vesicles and aging. Stem Cell Invest. *4*, 98.
27. Haji, M., Tanaka, S., Nishi, Y., Yanase, T., Takayanagi, R., Hasegawa, Y., Sasamoto, S., and Nawata, H. (1994). Sertoli cell function declines earlier than Leydig cell function in aging Japanese men. Maturitas *18*, 143–153.
28. Rebourcet, D., Wu, J., Cruickshanks, L., Smith, S.E., Milne, L., Fernando, A., Wallace, R.J., Gray, C.D., Hadoke, P.W.F., Mitchell, R.T., et al. (2016). Sertoli cells modulate testicular vascular network development, structure, and function to influence

circulating testosterone concentrations in adult male mice. Endocrinology *157*, 2479–2488.

29. Ma, W.-Y., Song, R.-J., Xu, B.-B., Xu, Y., Wang, X.-X., Sun, H.-Y., Li, S.-N., Liu, S.-Z., Yu, M.-X., Yang, F., et al. (2021). Melatonin promotes cardiomyocyte proliferation and heart repair in mice with myocardial infarction via miR-143-3p/Yap/Ctnnd1 signaling pathway. Acta Pharmacol. Sin. *42*, 921–931.
30. Zhang, W.R., Zhang, H.N., Wang, Y.M., Dai, Y., Liu, X.F., Li, X., Ding, X.B., and Guo, H. (2017). miR-143 regulates proliferation and differentiation of bovine skeletal muscle satellite cells by targeting IGFBP5. In Vitro Cell. Dev. Biol. Anim. *53*, 265–271.
31. Hall, I.F., Climent, M., Viviani Anselmi, C., Papa, L., Tragante, V., Lambroia, L., Farina, F.M., Kleber, M.E., März, W., Biguori, C., et al. (2021). rs41291957 controls miR-143 and miR-145 expression and impacts coronary artery disease risk. EMBO Mol. Med. *13*, e14060.
32. Zhang, P., Yang, W., Wang, G., and Li, Y. (2018). miR-143 suppresses the osteogenic differentiation of dental pulp stem cells by inactivation of NF-κB signaling pathway via targeting TNF-α. Arch. Oral Biol. *87*, 172–179.
33. Che, Y., Shi, X., Shi, Y., Jiang, X., Ai, Q., Shi, Y., Gong, F., and Jiang, W. (2019). Exosomes derived from miR-143-overexpressing MSCs inhibit cell migration and invasion in human prostate cancer by downregulating TFF3. Mol. Ther. Nucleic Acids *18*, 232–244.
34. Ma, W., Ding, F., Wang, X., Huang, Q., Zhang, L., Bi, C., Hua, B., Yuan, Y., Han, Z., Jin, M., et al. (2018). By targeting Atg7 MicroRNA-143 mediates oxidative stress-induced autophagy of c-Kit (+) mouse cardiac progenitor cells. EBioMedicine *32*, 182–191.
35. Lin, X.-T., Zheng, X.-B., Fan, D.-J., Yao, Q.-Q., Hu, J.-C., Lian, L., Wu, X.-J., Lan, P., and He, X.-S. (2018). MicroRNA-143 targets ATG2B to inhibit autophagy and increase inflammatory responses in Crohn's disease. Inflamm. Bowel Dis. *24*, 781–791.
36. Zhang, Z., Chen, C.-Z., Xu, M.-Q., Zhang, L.-Q., Liu, J.-B., Gao, Y., Jiang, H., Yuan, B., and Zhang, J.-B. (2019). MiR-31 and miR-143 affect steroid hormone synthesis and inhibit cell apoptosis in bovine granulosa cells through FSHR. Theriogenology *123*, 45–53.
37. Tanaka, T., Kanatsu-Shinohara, M., Lei, Z., Rao, C.V., and Shinohara, T. (2016). The luteinizing hormone-testosterone pathway regulates mouse spermatogonial stem cell self-renewal by suppressing WNT5A expression in Sertoli cells. Stem Cell Rep. *7*, 279–291.
38. Rivero-Müller, A., Potorac, I., Pintiaux, A., Daly, A.F., Thiry, A., Rydlewski, C., Nisolle, M., Parent, A.-S., Huhtaniemi, I., and Beckers, A. (2015). A novel inactivating mutation of the LH/chorionic gonadotrophin receptor with impaired membrane trafficking leading to Leydig cell hypoplasia type 1. Eur. J. Endocrinol. *172*, K27–K36.
39. Lee, J., Lee, H.C., Kim, S.-Y., Cho, G.J., and Woodruff, T.K. (2019). Poorly-controlled type 1 diabetes mellitus impairs LH-LHCGR signaling in the ovaries and decreases female fertility in mice. Yonsei Med. J. *60*, 667–678.
40. Gely-Pernot, A., Raverdeau, M., Célébi, C., Dennefeld, C., Feret, B., Klopfenstein, M., Yoshida, S., Ghyselinck, N.B., and Mark, M. (2012). Spermatogonia differentiation requires retinoic acid receptor γ. Endocrinology *153*, 438–449.
41. Chung, S.S.W., Wang, X., and Wolgemuth, D.J. (2009). Expression of retinoic acid receptor alpha in the germline is essential for proper cellular association and spermiogenesis during spermatogenesis. Development *136*, 2091–2100.
42. Zhang, S., Yu, M., Liu, C., Wang, L., Hu, Y., Bai, Y., and Hua, J. (2012). MIR-34c regulates mouse embryonic stem cells differentiation into male germ-like cells through RARg. Cell Biochem. Funct. *30*, 623–632.
43. Krieglstein, K., Miyazono, K., ten Dijke, P., and Unsicker, K. (2012). TGF-β in aging and disease. Cell Tissue Res. *347*, 5–9.
44. Luo, S., Shaw, W.M., Ashraf, J., and Murphy, C.T. (2009). TGF-ß Sma/Mab signaling mutations uncouple reproductive aging from somatic aging. PLoS Genet. *5*, e1000789.
45. Baugé, C., Girard, N., Lhuissier, E., Bazille, C., and Boumediene, K. (2014). Regulation and role of TGFβ signaling pathway in aging and osteoarthritis joints. Aging Dis. *5*, 394–405.
46. Luo, S., Kleemann, G.A., Ashraf, J.M., Shaw, W.M., and Murphy, C.T. (2010). TGF-β and insulin signaling regulate reproductive aging via oocyte and germline quality maintenance. Cell *143*, 299–312.
47. Liang, J., Tang, Y., Li, H., Mei, J., Cao, Z., Xia, H., Huang, R., Yang, Y., and Huang, Y. (2021). Isolation of Primary Leydig Cells from Murine Testis. Bio. Protoc. *11*, e4223.